Vertical mixing layer development

European Journal of Mechanics B/Fluids 43 (2014) 76–84

Contents lists available at ScienceDirect

European Journal of Mechanics B/Fluids

journal homepage: www.elsevier.com/locate/ejmflu

Vertical mixing layer development

Adam Robinson *, Jean-Baptiste Richon, Ian Bryden, Tom Bruce, David Ingram

Institute for Energy Systems, School of Engineering, The University of Edinburgh, King's Buildings, Mayfield Road, Edinburgh, EH9 3JL, United Kingdom

ARTICLE INFO

Article history:
Received 21 February 2013
Received in revised form
24 June 2013
Accepted 9 July 2013
Available online 17 July 2013

Keywords:
Turbulent mixing layer
Shear wave current
PIV

ABSTRACT

A new generation of current and wave testing tanks is required to simulate more realistic sea conditions at larger scales. One means of producing a current is by using groups of impellers arranged around the perimeter of a circular tank. Each propeller produces a single flow velocity which may be different to its neighbours. These differences can lead to a stepped or curved plan view velocity profile in the test section of the tank where a plug profile is required. It is important to understand what the maximum allowable velocity difference between each impeller can be before the required plug profile in the test section is compromised.

The situation where two individual fluid streams combine, leading to a turbulent mixing layer, is found in many applications and is therefore of great interest in wider fluid dynamics.

In the experimental work presented a setup is described which combines two water flows at different velocities to create a vertical shear. The evolution of the combined flow is studied using Particle Image Velocimetry (PIV). When analysed, these results lead to an understanding of various aspects of mixing layer flow recovery and how the bulk flow rates and velocity ratio affected them.

1. Introduction

Testing is an essential part of development for off-shore devices and structures. A current and wave testing tank capable of producing realistic sea conditions at 1:20 scale would provide a mid-step between existing small scale test facilities and sea trials.

One attractive method of producing a sea representative bulk fluid flow is to use the conditioned wake from a group of axial flow impeller inlets arranged around the perimeter of a circular tank. In Fig. 1, six separate perimeter inlets are combined to drive and remove fluid in a way that will form a one directional bulk flow. The aim of this is to create representative sea conditions, achieving a similar outcome to the tank design proposed by Salter [1]. This paper is concerned with the interaction between one flow stream and its neighbour. The creation of the bulk flow in a round tank will be detailed in a later work. The advantages of a round tank come not only from the ability to make a complex 3D bulk flow pattern but also from the generation and absorption of 3D waves. One problem with creating waves in a test tank is that there reflections bounce off solid surfaces such as walls and pass back through the test area. Two means exist to remove unwanted reflections from a wave tank. The first is to use the passive absorption of beaches, the second absorbing wave-makers [2]. A circular tank allows absorbing wave-makers to be used around the complete perimeter meter of the tank leaving no walls or corners to reflect waves, as detailed by Taylor et al. [3].

In the configuration shown in Fig. 1, each propeller inlet system produces a flow at a single velocity which may be different to its neighbours. These differences can lead to a stepped or curved plan view velocity profile in the test section of the tank, where a plug profile is usually required.

It is important for satisfactory operation of the proposed wave and current testing tanks that the maximum allowable velocity difference between fluid inlets is understood. If the difference in velocity is too great the required plug profile in the test section may be compromised. This will guide how many individual inlet systems are required for a given tank. In this work the wake evolution of the combined flow from two inlets will be studied in detail. Here the aim is to gain an understanding of the recovery of the turbulent flow downstream of the flow combination for conditions relevant to wave and current testing tanks.

To investigate the wake evolution, an experimental setup was created which combines two flows at different velocities to create a vertical shear (Fig. 2). The flow downstream of the stream combination was measured using Particle Image Velocimetry (PIV). Due to the orientation of the existing flume, on which this experiment is based, the shear layer tested here is vertical. In a combined current and wave testing tank (Fig. 1) the shear layer would be horizontal. As density effects are negligible in this case the results should be comparable regardless of orientation.

Although this work has an application for current and wave testing tank design, fluid combining to form a turbulent mixing layer is a classic fluid dynamic case, which can be seen in nature and many engineered flows.

* Corresponding author. Tel.: +44 01316513575.
E-mail address: adam.robinson@ed.ac.uk (A. Robinson).

0997-7546/$ – see front matter © 2013 Elsevier Masson SAS. All rights reserved.
http://dx.doi.org/10.1016/j.euromechflu.2013.07.001

Nomenclature

u	Mean velocity in the x direction (m/s)
u_h	Mean velocity in the x direction for the high speed side (m/s)
u_l	Mean velocity in the x direction for the low speed side (m/s)
R	Velocity ratio $= \frac{u_l}{u_h}$

2.1. Turbulent mixing layers

Turbulent mixing layers are an important and well studied phenomenon in fluid dynamics. They are found in nature in atmospheric and ocean flows as well as in engineered situations. Turbulent mixing layers are a significant source of aero-acoustic noise and understanding them is of importance to aerospace design [4]. Mixing layers are also present in chemical plants and are critical to increase mixing performance [5,6]. This mixing situation also lends itself to pure fluid dynamic study and model validation due to the absence of bounding walls and rapid but measurable growth of turbulent structures [7].

When two fluid streams of different velocities combine an energy imbalance exists. The faster stream transfers momentum to the slower stream until there is equality. The factors that affect the time and distance required to achieve an energy balance include [7]:

- Overall flow speed.
- The ratio of velocity between the two streams.
- The initial condition.
- Fluid properties.
- Test section geometry and size.
- Flow splitter geometry and size.
- Splitter plate boundary layer state.
- Free stream turbulence level.

If the velocity difference is low enough, the energy will be transferred through laminar viscous forces. Once a certain threshold is reached, the flow will transition to a turbulent behaviour resulting in eddies at the stream interface; in this regime many distinct behaviours have been observed.

Loucks and Wallace [6] state that the turbulent mixing layer is initiated by a Kelvin–Helmholtz instability developing after the splitter plate, resulting in a 2D span-wise series of vortical structures known as rollers (Fig. 3).

The rollers grow in size as they travel downstream and are relatively evenly spaced when they begin to join and interact with each other (Loucks and Wallace [6]). Brown and Roshko [8] observed that when the mixing layers are maintained the vortex layer is sustained a long way from the splitter plate. However, in a situation like the one investigated here, where the mixing layers are allowed to equalise, the roller structures eventually break down into disorganised turbulent flow.

Rollers have been observed through a range of Reynolds numbers from low values (RE $= 1.5 \times 10^4$) [9] to high values (RE $= 2 \times 10^5$) [10]. Browand and Latigo [11] suggested rollers are universally present for turbulent mixing layers. However Chandrsuda et al. [12] later found that if the free-stream turbulence is high enough rollers will not form.

Browand and Troutt [9] observed that although the rollers are largely a 2D span-wise phenomenon downstream roller interaction leads to some 3D effects. Jimenez [13] reported that these span-wise effects can influence roller behaviour as well as mixing rates. High free-stream turbulence was found to reduce how far downstream the rollers would exist (Chandrsuda et al. [12]).

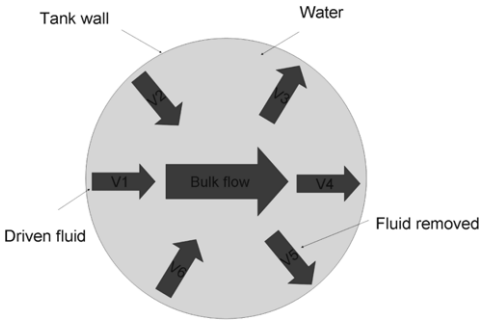

Fig. 1. Current generation in a tank viewed in a direction aligned with gravity.

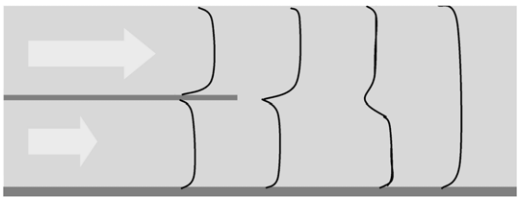

Fig. 2. A 2D slice of separate streams of driven fluid combining to form a bulk flow in a flume viewed from the side with gravity aligned down the page. Black lines indicate the type of velocity profile development expected.

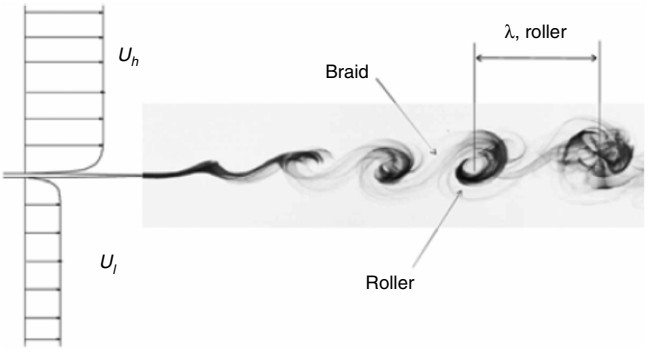

Fig. 3. Turbulent mixing layer diagram, from Loucks and Wallace [6].

Mehta [14] investigated how the ratio between the average velocities of the low speed and high speed inlets affected the development of turbulent mixing layers. Mehta [14] found that as the two streams became similar in speed the splitter plate wake dissipation distance extended downstream. Mehta [14] also noted that increased velocity difference increases entrainment and reduces splitter plate wake dissipation distance. These findings were later supported by Azim and Islam [7].

Azim and Islam [7] state that turbulent mixing layer behaviour is highly sensitive to the physical conditions and geometry which makes comparison to, and repetition of, previous works difficult.

Many works compare in some parameters but not others. For example, Azim and Islam [7] test at similar velocity ratios to those present in a current and wave testing tank, but use air as a medium as well as having significant differences in splitter plate geometry and free stream Reynolds numbers. An example of a water flume is given by Guo et al. [5], who investigate flows with far higher velocity differences than those tested here. The high sensitivity of turbulent mixing layers to physical conditions and geometry, along with there being no previous studies with similar conditions to those of interest here mean that it is prudent to perform a new experiment.

The measurement and visualisation of turbulent mixing layers have been done in many ways depending on the aim of the study and the technology available. To gain understanding of the underlying physical processes, visualisation has been useful with early

works using smoke [12] and chemical reactions which highlight areas of high mixing with a visible reaction product [15]. Point measurements of velocity have been used to construct flow maps of average data and to quantify turbulence. Point measurement techniques used for turbulent mixing layers include pitot tubes [16], hot-wire anemometry [6,14,17] and Laser Doppler Anemometry [18]. PIV is capable of measuring velocities over a large area instantaneously and therefore aiding the investigation of turbulent mixing layers. Guo et al. [5] used a 2D PIV system to produce instantaneous vector and contour velocity plots in which a series of rollers can be seen. Along with the visualisation of the rollers, Guo et al. [5] use PIV to provide an efficient method of obtaining distributions of Reynolds stresses and other flow quantities.

Two related papers where PIV has been used to investigate the turbulent mixing of a confined planar-jet are: Feng et al. [19] and Liu et al. [20]. This situation is comparable with a turbulent mixing layer with two shear layers separated by coherent eddies.

To provide a means of predicting and investigating the behaviour of a turbulent mixing layer without having to create a representative experiment, many numerical models have been created. Balaras et al. [21] suggest that for turbulent mixing layers, which are very sensitive to small upstream changes, numerical simulations have the benefit of being able to precisely define inputs and the environment when compared to physical experiments.

The typical turbulent mixing layer involves large vortical structures, which eventually break down to the Kolmogorov scale before dissipating due to viscous effects. This breakdown is physically complex and therefore requires powerful numerical techniques to produce a representative simulation.

Before the development of PIV there was no experimental method capable of capturing a large area containing several rollers. It was possible to visualise rollers without velocity data or use point data and then try and recreate a picture of the roller behaviour with sequential velocity point data. With only these options before PIV, numerical methods provide an attractive method of acquiring this type of data.

Useful simulations of turbulent mixing layers have been performed analytically by Neu [22] and, using Lagrangian numerical methods by Ashurst and Meiburg [23]. However methods that provide instantaneous planes of velocity data, typically involve numerical solutions of the Navier–Stokes equations either by Direct Numerical Simulation (DNS) or Large-Eddy Simulation (LES). DNS attempts to solve the Navier–Stokes equations for all scales of motion whereas LES only represents motion larger than a given scale and models the effects of the smaller eddies.

Simulations have provided insights into rollers, braid physics (Fig. 3) and roller–roller interaction as well as giving information on energy distribution within the coherent structures [24,25].

An example of DNS being used to simulate a turbulent mixing layer is provided by Rogers and Moser [24,25]. LES simulations were performed by Comte et al. [26] and Bogey, Bailly and Juvé [27]. There are no examples of a Reynolds Averaged Navier–Stokes (RANS) model being employed to simulate turbulent mixing layers. However, Feng et al. [19] and Liu et al. [20] use it for a related jet flow.

The need for this work comes from:

- The lack of published simulations or experiments that investigate more than twenty roller diameters downstream of the splitter plate.
- The behaviour of turbulent mixing layers is very sensitive to the flow conditions and geometry and therefore it is prudent to perform an experiment where these parameters differ significantly from those tested before.
- A lack of experimental work in the parameter range of interest to combined wave and current tanks.
- The need to aid the design of combined wave and current tanks as well as the development and validation of numerical design tools.

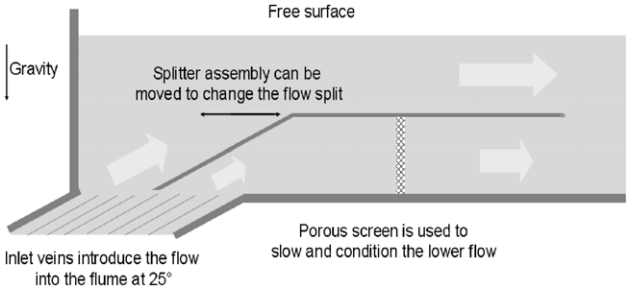

Fig. 4. A 2D slice of the experimental setup.

3.1. Experimental facility

In order to create two separate flows at different velocities that can be recombined in order to study wake evolution (Fig. 2) an existing water flume was modified. A single flow is selectively split into two then separated by a wall; one half is then slowed down and conditioned by a porous screen as illustrated in Fig. 4. This setup is the same concept to that used by Guo et al. [5] and Loucks et al. [6] among others.

To further control the velocity ratio, the splitter assembly can be slid forward, altering the flow distribution. The flume walls are constructed with painted plywood with one side wall being glass to allow PIV measurement. The geometry is shown in Fig. 5.

Typically, splitter plates are tapered to a sharp point or are made as thin as possible. In this work due to the application, the splitter plate end is rounded and relatively thick at 18 mm. This rounding is representative of the splitter walls used in a large combined wave and current tank which cannot have ends that taper to a sharp point due to how the tank is made. Although tripping the boundary layer before the end of the splitter plate has been shown to increase the mixing rate [28] and could be useful in the final application, it is not done in this experiment.

The flume is mounted alongside the observation window of a large wave testing tank with water drawn from the tank into the flume using an electrically driven impeller. Swirl removal and conditioning is provided by honeycomb material mounted directly after the propeller. Once the water has passed through the flume it exits into the wave tank. The flume was run for a sufficiently long time before measurements were taken to ensure no start-up transience was recorded.

Guo et al. [5] highlighted that surface waves affected the development of the mixing layer. In these experiments the free surface was lifted slightly ($<$2 mm) near the inlet but no significant surface waves were observed.

For these tests the propeller is set at three different speeds which determine the total flow rate. Three settings are also used for the flow split giving nine different test conditions.

3.2. Measurement setup

A 2D Particle Image Velocimetry system was used for the experimental setup shown in Fig. 6. Images were collected with a Sensicam QE CCD camera with a 1376 $\times$ 1040 pixel resolution, 12 bit monochrome image output, frame rate up to 10 images/s, fitted with a 55 mm/f2.8 Macro lens. With a stand-off distance of 300–310 mm to the glass wall of the channel, this arrangement produced a field of view of 200 mm (x) by 300 mm (y).

The image plane was illuminated by a pulsed dual-cavity Nd:YAG laser with energy of 200 mJ at 532 nm and a maximum repetition rate of 15 Hz for each cavity (new Wave Research Solo PIV 200XT). This was coupled to an adjustable focus lens assembly to generate a divergent light sheet. The focusing element was set so that the waist of the light sheet was positioned approximately

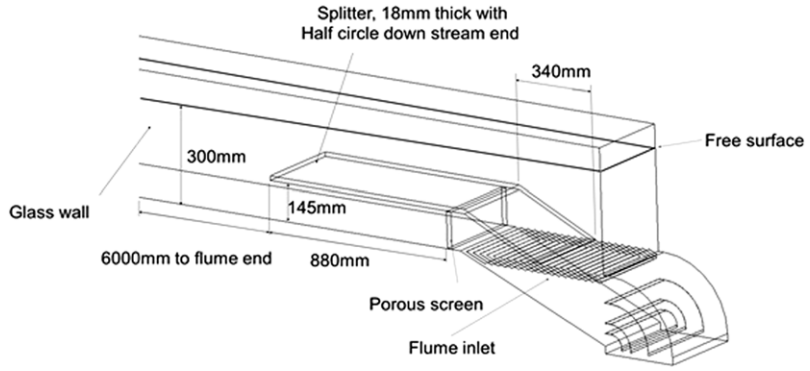

Fig. 5. Experimental setup.

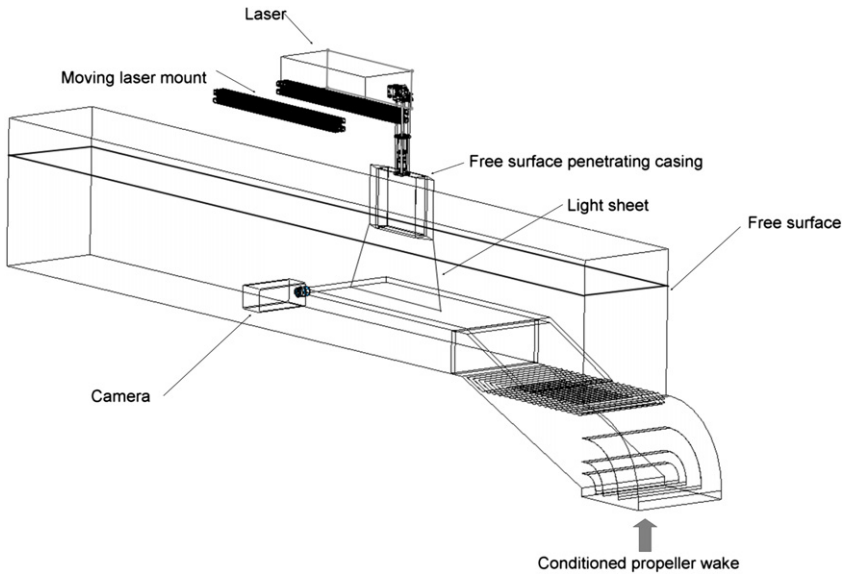

Fig. 6. Measurement setup.

mid-depth in the channel. A light sheet thickness of 1 mm was used throughout.

The light sheet penetrated the free surface of the water through the bottom of a stream-lined polycarbonate casing which provided stable optical access to the flow. The depth of immersion of the casing was kept as small as possible to minimise flow disturbance whilst ensuring the bottom surface was always in contact with water only. The flow was seeded with polyamide particles with an average diameter of 10 μm and density of 1050 kg/m^3. For the purpose of this study the particle buoyancy was sufficiently close to neutral for buoyancy forces and slippage to be considered negligible in comparison to forces generated by fluid motion.

Image scaling and positioning was achieved using a calibration target with a pattern of regular points at known dimensions. This target was imaged using the experimental setup before and after each image set. This insured that correct positions and particle displacements could be assigned during image processing.

The camera and laser were synchronised using a programmable pulse generator (EG32, R&D Vision).

A Series of 500 image pairs per case per position were acquired at a frame rate of four images per second and later analysed with the PIVView 2D software package (Pivtec GmbH).

The algorithm used to interrogate the image pairs uses grid refinement and iterates three times. Interpolation is done using a third order B-Spine method with outliers being filtered out using set pixel displacements. Particle centres are measured to a sub pixel accuracy using a 3^2 least square Gauss fit.

3.3. Experimental uncertainty

The geometrical tolerance of the experimental rig was less than ± 1 mm with the measurement setup manufactured to ± 0.1 mm.

The accumulated uncertainty for the velocity measurements for a PIV system is typically $\pm 5\%$ [29]. Here to minimise the error, the experiment was set up in the way outlined by Westerweel [30]. An average pixel displacement of 6 pixels was maintained throughout. Following the 1/4 rule, assuming a maximum measurement error of 0.1 pixels [30] for a 24^2 interrogation region with 50% overlap, the displacement error should be 0.1/12 of full scale and therefore below 1%.

Temperature remained at 16 °C throughout the tests and was measured using a thermometer with an accuracy of ± 0.5 °C.

The x positions for the images were reassembled using the calibration target fixed in a known position measured by rule and was ± 1 mm or better. The y position was more accurate, as the calibration target sat on the bottom of the flume and, therefore, the position could be determined through image processing, resulting in an accuracy of better than ± 0.2 mm.

4. Results

To provide a series of results an experimental rig was set up with three different velocity ratios at three total flow rates. The details of these tests are described in Table 1.

Table 1
Test cases.

Case	u (m/s)	u_h (m/s)	u_l (m/s)	R	Initial location x (mm)	Roller size (mm)	Dip recovery position x (mm)	Split ratio far-field	Far-field position x (mm)	Initial min u location y (mm)
1A	0.38	0.52	0.29	0.56	29.5	48.0	132	0.25	930	175
1B	0.37	0.50	0.29	0.57	104	47.0	144	0.22	931	170
1C	0.38	0.50	0.30	0.60	21.7	42.1	N/A	0.20	894	171
2A	0.46	0.63	0.35	0.56	27.2	48.2	137	0.25	930	176
2B	0.45	0.61	0.35	0.58	102	47.6	123	0.22	931	172
2C	0.44	0.56	0.37	0.65	159	48.6	N/A	0.17	983	170
3A	0.62	0.84	0.48	0.57	22.5	49.7	135	0.26	930	177
3B	0.58	0.78	0.46	0.59	125	52.2	139	0.23	931	176
3C	0.59	0.78	0.48	0.62	21.7	55.2	158	0.17	979	172

Table 2
Splitter wake dissipation position for selected cases.

Case	u (m/s)	Velocity ratio initial	Splitter wake dissipation position x (mm)
1A	0.38	0.56	19
1C	0.38	0.60	27.2
3A	0.62	0.57	14.5
3C	0.59	0.62	25

The second column in Table 1 gives the average speed from the free surface to the bottom wall of the flume which should be uniform at any stream-wise location. The next three columns give the average velocity above u_h and below u_l the splitter along with the velocity ratio $R = u_l/u_h$. These velocities were taken as close to the splitter as possible whilst maintaining an acceptable level of accuracy. Therefore the fourth column is the x position, where the initial values are taken.

The fifth column is the average roller diameter measured within 150 mm of the splitter.

The dip recovery position refers to the first x position, where the dip caused by the flow combination is no longer measurable.

The far field velocity ratio gives an indication of the flow recovery and is taken at a location close to the downstream end of the measured area given in the penultimate column.

The last column gives the y position of the lowest velocity in the dip close to the splitter plate in each case.

Although the change in R may appear to be relatively small it is enough to create measurable differences in flow behaviour in terms of development distance (Table 1) and roller behaviour (Section 4.1). These changes in behaviour would be sufficient for model validation.

The range of R was chosen to match that required for a circular combined current and wave testing tank with twenty eight inlets arranged around the perimeter as shown in Fig. 1.

In most studies of turbulent mixing layers [5,14,31], the results are non-dimensionalised or normalised, typically using an average velocity and the initial roller diameter or splitter plate boundary layer thickness. This is because in the conditions tested by others, there has been a constant stream of regular rollers. Here although the diameter is consistent, the rollers are not always continuous. There is also an error as large as 6% in the measurement of roller diameter as detailed in Section 4.1. To use roller diameter to non-dimensionalise here may lead to erroneous comparisons.

4.1. Analysis

The first thing to observe is that the experimental arrangement allows the creation of turbulent mixing layers with initial velocity ratios between 0.55 and 0.65, with bulk average flow velocities between 0.37 and 0.62.

A comparison between the initial velocity ratio and far field ratio shows that the flow does not recover fully in any case within the measured section.

Downstream from where the two streams join after the splitter plate there is a region where the velocity drops to zero and a dip is evident in the velocity profile. This dip can be seen in the graph for $x = 22.5$ in Fig. 12. Due to the fact that PIV gives full coverage of the test area it is possible to measure where this dip is recovered. The dip recovery position seems to be unaffected by the bulk average velocity and therefore it is possible that the dip recovery position is geometry-dependent. The effect of a decrease in velocity ratio is a decrease in dip recovery distance. This trend is probably due to increased energy transfer between the two streams. Guo et al. [5], Mehta [14] and Liu et al. [20] reported a negative velocity directly after the splitter plate. However, this dissipates quickly and can only be seen here where the PIV measurement area was close to the splitter plate (Figs. 12 and 13). Table 2 gives the splitter plate wake dissipation distance, along with the flow parameters.

Guo et al. [5] reported that, for the conditions tested, the splitter plate dissipation distance was 28 mm and was similar for all cases tested. Guo et al. [5] varied only the bulk velocity whilst maintaining a constant velocity ratio. From the results shown in Table 2, it is evident that the velocity ratio has a far greater effect on when the splitter plate wake dissipates than the bulk velocity, supporting the findings of Guo et al. [5].

Mehta [14] varied the velocity ratio and found the same relationship. Mehta [14] added that as the two streams became similar in speed, the splitter plate wake dissipation distance extended further than the measured test area.

An effect that has not been investigated before is the position of the lowest velocity of the dip in the non stream-wise (y) direction relative to the splitter plate centre ($y = 172$ mm). From the results produced here it is evident that, at higher velocity ratios, the lowest velocity sits at the centre of the line given by the centre of the splitter plate and that, as the velocity ratio drops, it moves towards the higher speed side as visualised in Fig. 7.

The PIV setup created a large grid of simultaneous velocity data, which can be used to identify and measure rollers. To visualise the rollers best, the velocity data was converted to vector maps and the mean flow velocity was subtracted. In previous investigations a continuous roller–braid–roller structure was found after the splitter plate as shown in Fig. 3. In the conditions tested here three different behaviours could be visualised from the five hundred vector maps for each case.

Only in the Cases 3A, 3B, 1B, and 1A, where the velocity ratios approached the maximum, was there strong visual evidence of a series of rollers being produced in the manner found before (Fig. 8).

In Cases 3C, 2A and 2B, one strong roller was produced after the splitter and then no other clear following rollers were evident (Fig. 9).

In the remaining cases, 2C and 1C, the creation of a clear roller was intermittent and not evident in every vector map.

The method of estimating roller diameter used here was to measure them directly off the vector maps using the PIV software, which leads to errors. The error comes from the fact that for each vector arrow an 8×8 pixel square is analysed. The edge of the roller

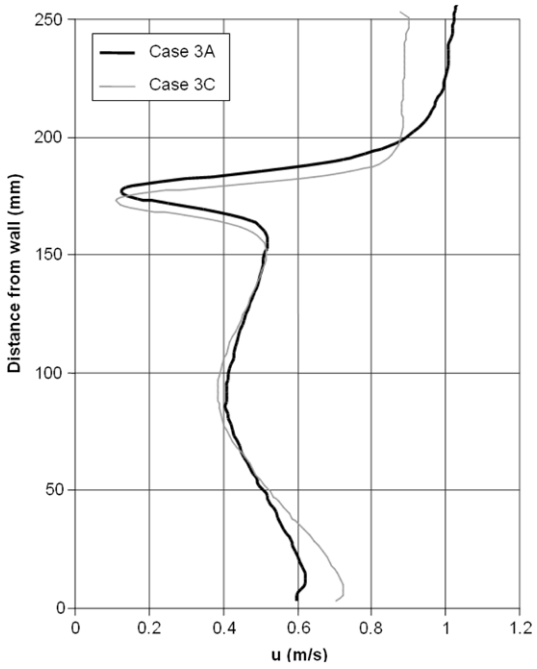

Fig. 7. Velocity profile comparison for Case 3A ($x = 21.5$ mm) and Case 3C ($x = 33.3$ mm).

can be estimated by vector size and direction so an error of 8 pixels is possible on each side of the roller. The total error can be as large as 3 mm for a 42 mm roller. To minimise error and give a more time averaged roller diameter for each case ten rollers were measured then the value is averaged. This value is given in Table 1. Rollers are only approximately round as they are continually expanding; this can be seen in shadowgraph images such as those presented by Brown and Roshko [8].

From the general time averaged results in Table 1, it is clear that the change in roller size is not that large with either change in velocity ratio or bulk flow rate. Due to the changes being of a magnitude close to the error, it is not useful to comment on any trends.

Velocity profiles at various positions down the flume for four cases (1A, 1C, 3A and 3C) are provided in Figs. 12 and 13. Along with mean velocity profiles a measure of turbulence is provided with turbulent intensity. Turbulent intensity is given by the ratio of the standard deviations of velocity and mean velocity. The other five cases (1B, 2A, 2B, 2C and 3B) followed the same development trend and therefore velocity profiles are not provided. However general data for these cases is available in Table 1.

From the graphs in Figs. 12 and 13, it is evident that general behaviour is similar in all cases. For a short distance downstream of the plate there is a dip in velocity around the centre of the splitter plate. Further away from the plate, the velocity profile flattens and develops as expected. One observation is that the effect of the joining at the splitter plate is still visible in the turbulent intensity profiles far longer than in the velocity profiles. For case 3C the dip in the velocity profile is gone by $x = 158$ mm where the dip in the turbulent intensity profile is still visible at $x = 300$ and can be seen in Fig. 12.

This underlying turbulent zone would affect the recovery rate in a way that may not be explained without the turbulence data.

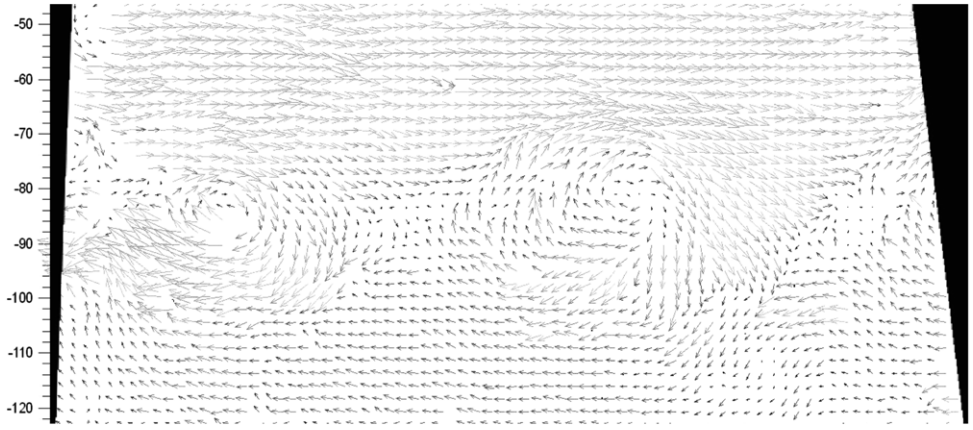

Fig. 8. A vector map of the *xy* plane for Case 3A directly after splitter with the mean velocity subtracted. The scale on the left is in mm.

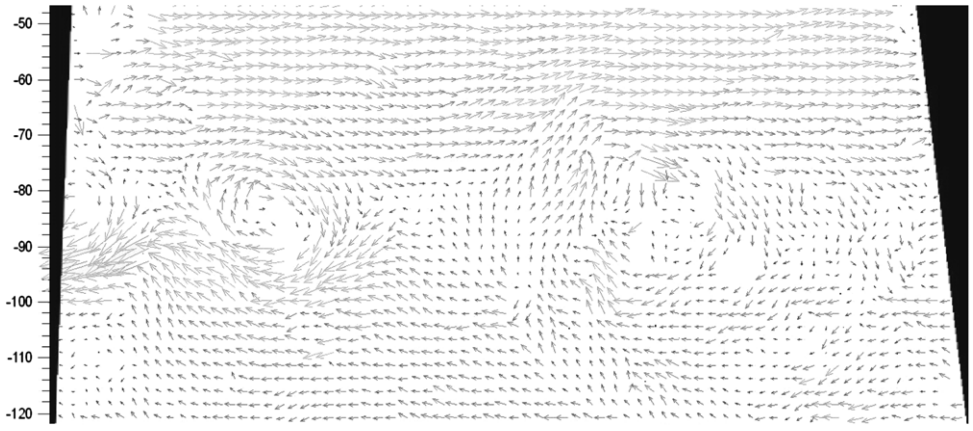

Fig. 9. A vector map of the *xy* plane for Case 2A directly after splitter with the mean velocity subtracted. The scale on the left is in mm.

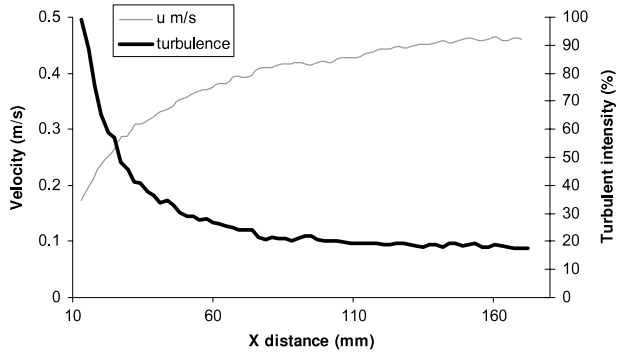

Fig. 10. Recovery rate graph for Case 3A at splitter centre ($y = 172$).

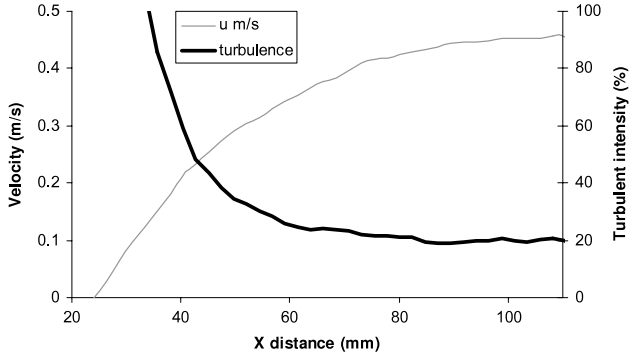

Fig. 11. Recovery rate graph for Case 3C at splitter centre ($y = 172$).

The turbulence decays and recovers far more quickly than the velocity and is almost fully-developed within the test area unlike the velocity. The only exception to this is the dip region which has a slower rate of recovery.

Mehta [14] found that mixing layer growth was linear once the splitter wake had dissipated. Here the general trend is the same as can be seen in Figs. 10 and 11. This is especially evident in the decay of turbulent intensity. Here the beginning of a linear region does not directly correlate with the splitter wake dissipating for the conditions tested.

Mehta [14] also stated that growth rate was reduced when the difference between the velocities decreases. This matches the results presented here when examining the gradient in Figs. 10 and 11 as well as for cases 1A and 1C.

5. Conclusions

An investigation of the behaviour of turbulent mixing layers caused by the shear between two streams was conducted. Conditions were set to match those seen in a water filled current and wave testing tank.

The results extend further downstream of the flow combination point than in previous studies although the setup length remains insufficient to observe full flow recovery. The wake is measured using PIV and gives a large grid of simultaneous velocity data that has been used both for the identification of flow structures and quantification of the flow.

The experimental setup allowed testing of the effects of both bulk flow rate and the velocity difference between the streams in the development of the flow. From this the following conclusions can be drawn:

- The recovery distance of the dip that occurs where the streams combine seems to be unaffected by the bulk average velocity. Therefore dip recovery position might be geometry dependent.

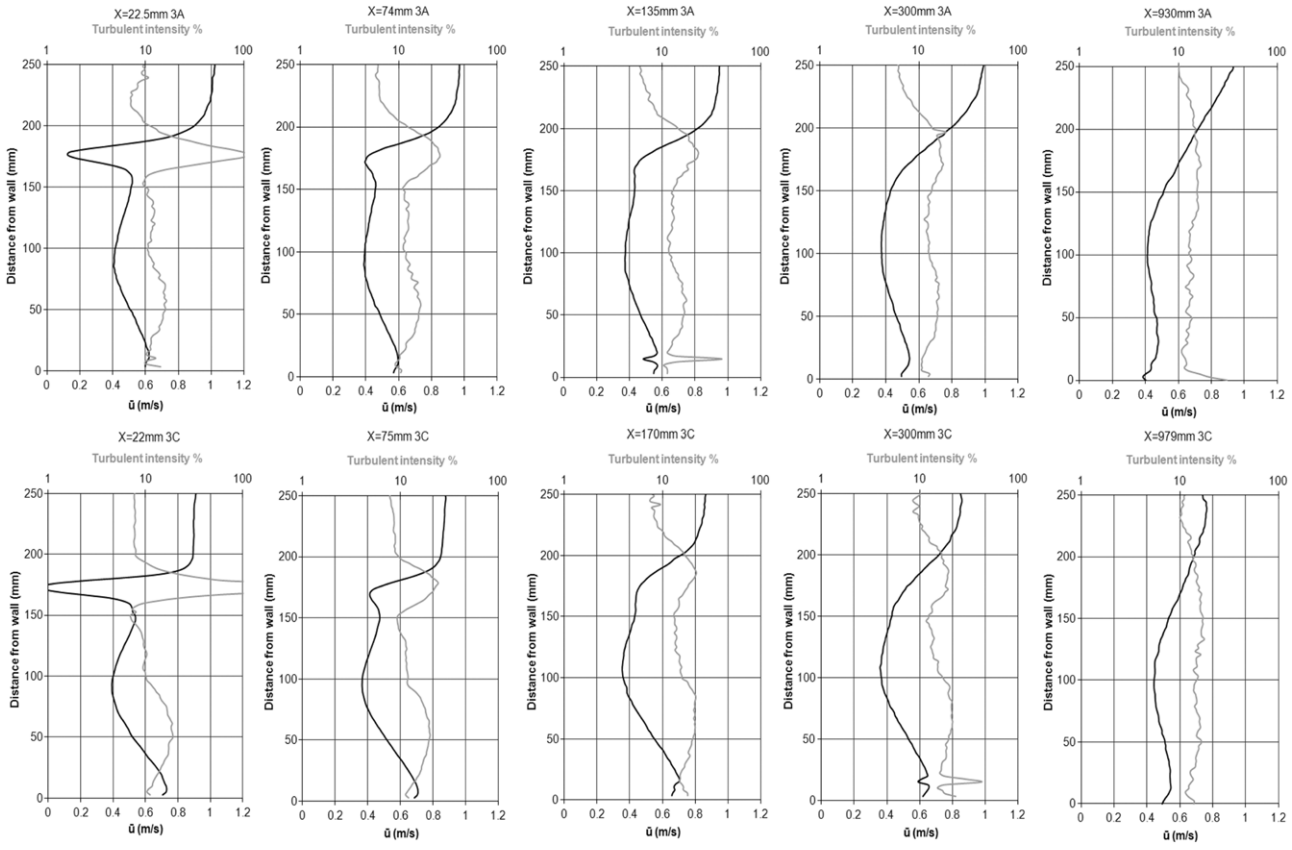

Fig. 12. Mean velocity u versus distance from the wall for various X positions, for Case 3A and 3C. The grey line is turbulent intensity and the black is velocity.

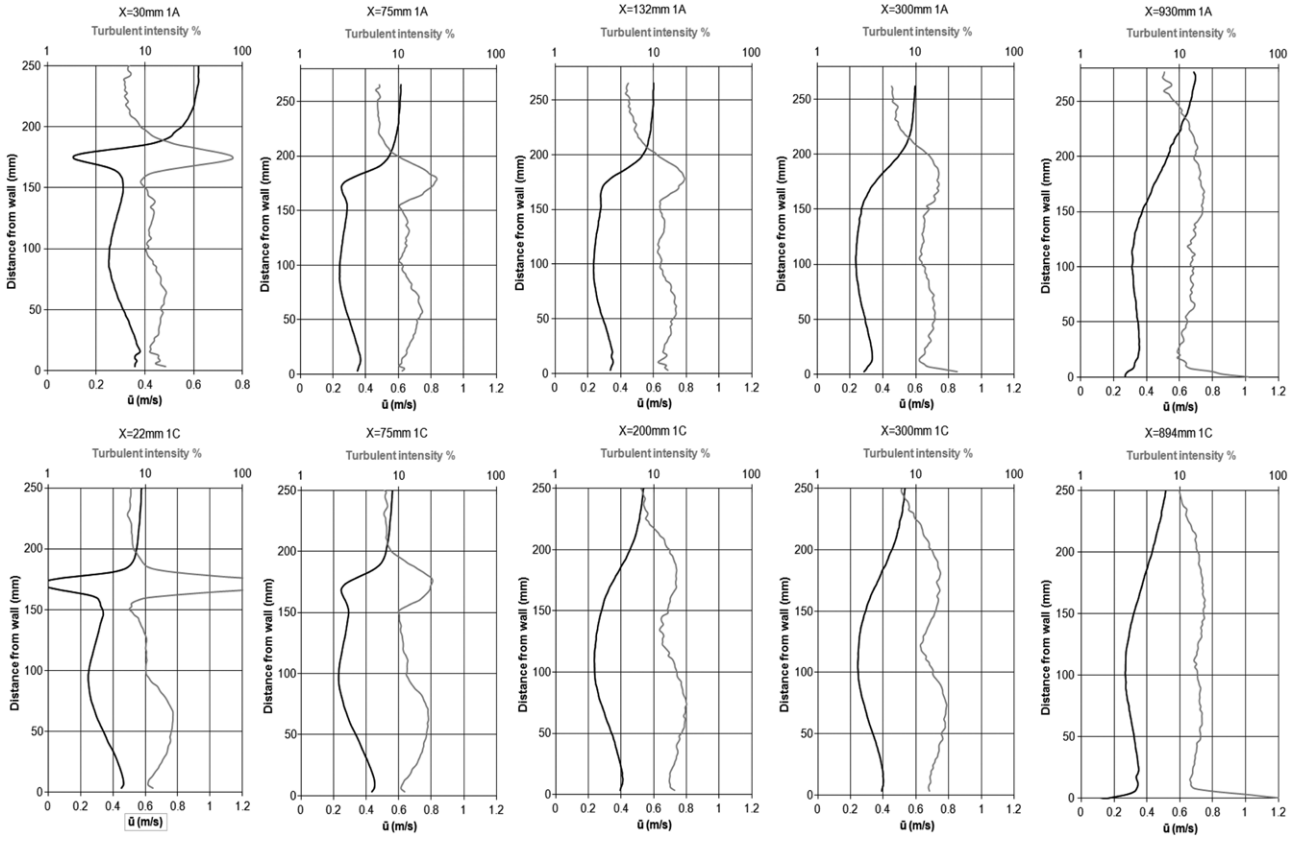

Fig. 13. Mean velocity u versus distance from the wall for various X positions for Case 1A and 1C. The grey line is turbulent intensity and the black is velocity.

- The effect of decreasing velocity ratio is to decrease dip recovery distance.
- Velocity ratio has a far larger effect on the dissipation of the splitter plate wake than the bulk velocity.
- For the higher velocity ratios the point of the velocity profile dip sits at the centre of the line given by splitter plate. As the velocity difference between the streams increases the dip moves towards the higher speed size.
- Through visualisation three distinct roller behaviours can be observed depending on the conditions present.
- The turbulence decays and recovers earlier downstream than the velocity profile.
- Splitter plate wake recovery follows a curved trend for a short distance, and then becomes linear, with the recovery rate reducing when the difference between the velocities decreases.

Along with the insight into the phenomena at work the results presented here will support the development and validation of numerical models.

The next stage of this work is to develop accurate and economical simulations of the evolution of the shearing flow described in this paper. Once this method is validated it will be extended to provide a numerical model of the plan view flows in a 3D combined current and wave tank. It is hoped that this model will provide a useful design tool and a means to test inlet flow control scenarios.

Acknowledgement

The authors would like to thank the Engineering and Physical Science Research Council for funding this research [EP/H012745/1].

References

[1] S.H. Salter, Design and construction of a 360-degree flow table with control of velocity gradient, IGR Report to EPSRC GR/R20694/01, 2003.
[2] S.H. Salter, Absorbing wave-makers and wide tanks, in: Directional Wave Spectra Applications, Am. Soc. Civ. Eng, Berkeley, 1981.
[3] J.R.M. Taylor, M. Rea, D.J. Rogers, The Edinburgh curved tank, in: 5th European Wave Energy Conference, Cork, Ireland, 2003.
[4] T.I.M. Colonius, S.K. Lele, P. Moin, Sound generation in a mixing layer, J. Fluid Mech. 330 (1997) 375–409.
[5] F. Guo, et al., Investigation of turbulent mixing layer flow in a vertical water channel by particle image velocimetry (PIV), Can. J. Chem. Eng. 88 (6) (2010) 919–928.
[6] R.B. Loucks, J.M. Wallace, Velocity and velocity gradient based properties of a turbulent plane mixing layer, J. Fluid Mech. 699 (2012) 280–319.
[7] M. Azim, A. Islam, Plane mixing layers from parallel and non-parallel merging of two streams, Exp. Fluids 34 (2) (2003) 220–226.
[8] G.L. Brown, A. Roshko, On density effects and large structure in turbulent mixing layers, J. Fluid Mech. 64 (04) (1974) 775–816.
[9] F.K. Browand, T.R. Troutt, A note on spanwise structure in the two-dimensional mixing layer, J. Fluid Mech. 97 (04) (1980) 771–781.
[10] M.D. Slessor, C.L. Bond, P.E. Dimotakis, Turbulent shear-layer mixing at high Reynolds numbers: effects of inflow conditions, J. Fluid Mech. 376 (1998) 115–138.
[11] F.K. Browand, B.O. Latigo, Growth of the two-dimensional mixing layer from a turbulent and nonturbulent boundary layer, Phys. Fluids 22 (6) (1979) 1011–1019.
[12] C. Chandrsuda, et al., Effect of free-stream turbulence on large structure in turbulent mixing layers, J. Fluid Mech. 85 (04) (1978) 693–704.
[13] J. Jimenez, A spanwise structure in the plane shear layer, J. Fluid Mech. 132 (1983) 319–336.
[14] R.D. Mehta, Effect of velocity ratio on plane mixing layer development: influence of the splitter plate wake, Exp. Fluids 10 (4) (1991) 194–204.
[15] R. Breidenthal, Structure in turbulent mixing layers and wakes using a chemical reaction, J. Fluid Mech. 109 (1981) 1–24.
[16] P. Bradshaw, The effect of initial conditions on the development of a free shear layer, J. Fluid Mech. 26 (2) (1966) 225–236.
[17] J.M. Wallace, P.V. Vukoslavcevic, Measurement of the velocity gradient tensor in turbulent flows, Annu. Rev. Fluid Mech. 42 (1) (2010) 157–181.
[18] D.B. Lang, Laser Doppler Velocity and Vorticity Measurements in Turbulent Shear Layers, California Institute of Technology, 1985.

[19] H. Feng, et al., Investigation of turbulent mixing in a confined planar-jet reactor, AIChE J. 51 (10) (2005) 2649–2664.
[20] Y. Liu, et al., Turbulent mixing in a confined rectangular wake, Chem. Eng. Sci. 61 (21) (2006) 6946–6962.
[21] E. Balaras, U.G.O. Piomelli, J.M. Wallace, Self-similar states in turbulent mixing layers, J. Fluid Mech. 446 (2001) 1–24.
[22] J.C. Neu, The dynamics of stretched vortices, J. Fluid Mech. 143 (1984) 253–276.
[23] W.T. Ashurst, E. Meiburg, Three-dimensional shear layers via vortex dynamics, J. Fluid Mech. 189 (1988) 87–116.
[24] M.M. Rogers, R.D. Moser, The three-dimensional evolution of a plane mixing layer: the Kelvin–Helmholtz rollup, J. Fluid Mech. 243 (1992) 183–226.
[25] M.M. Rogers, R.D. Moser, Direct simulation of a self-similar turbulent mixing layer, Phys. Fluids 6 (1994) 903–923.
[26] P. Comte, J.H. Silvestrini, P. Guo, Streamwise vortices in Large-Eddy simulations of mixing layers, Eur. J. Mech. B Fluids 17 (4) (1998) 615–637.
[27] C. Bogey, C. Bailly, D. Juve, Numerical simulation of sound generated by vortex palring in a mixing layer, AIAA J. 38 (2000) 2210–2218.
[28] M.W. Plesniak, J.H. Bell, R.D. Mehta, Effects of small changes in initial conditions on mixing layer three-dimensionality, Exp. Fluids 14 (4) (1993) 286–288.
[29] G.F. Oweis, et al., Development of a tip-leakage flow—part 1: the flow over a range of Reynolds numbers, J. Fluids Eng. 128 (4) (2006) 751–764.
[30] J. Westerweel, Fundamentals of digital particle image velocimetry, Meas. Sci. Technol. 8 (12) (1997) 1379–1392.
[31] N. Li, E. Balaras, J. Wallace, Passive scalar transport in a turbulent mixing layer, Flow Turbul. Combust. 85 (1) (2010) 1–24.